Scientific Research Publishing

Materials Sciences and Applications, 2026, 17(9), 241-253
https://www.scirp.org/journal/msa
ISSN Online: 2153-1188
ISSN Print: 2153-117X

Effect of Anodic Coating Thickness on the Corrosion Behavior of AA6005 Aluminum Alloy in a Simulated Acid Rain Environment

Eren Saray[1], Mesut Yıldız[2], Fatma Zehra Arı[1], Demet Giyik[1], Hüsnü Gerengi[1]

[1]Corrosion Research Laboratory, Department of Mechanical Engineering, Faculty of Engineering, Düzce University, Düzce, Türkiye
[2]Department of Mechanical and Metal Technologies, Dr. Engin Pak Cumayeri Vocational School, Düzce University, Düzce, Türkiye
Email: ernsry@gmail.com, fatmaari912@gmail.com, demetgiyik976@gmail.com, husnugerengi@gmail.com, mesutyildiz@duzce.edu.tr

How to cite this paper: Saray, E., Yıldız, M., Arı, F.Z., Giyik, D. and Gerengi, H. (2026) Effect of Anodic Coating Thickness on the Corrosion Behavior of AA6005 Aluminum Alloy in a Simulated Acid Rain Environment. *Materials Sciences and Applications*, **17**, 241-253.
https://doi.org/10.4236/msa.2026.179016

Received: July 28, 2026
Accepted: September 13, 2026
Published: September 16, 2026

Abstract

Atmospheric acid rain significantly accelerates the deterioration of aluminum alloys used in outdoor structures, emphasizing the importance of optimized anodic oxide coatings for AA6005 aluminum alloy. This study investigated the corrosion behavior of uncoated and anodized AA6005 specimens with coating thicknesses of 10 μm and 14 μm in a simulated acid rain solution using electrochemical techniques combined with post-exposure surface characterization. Open circuit potential (OCP), electrochemical impedance spectroscopy (EIS), and Tafel polarization tests revealed that anodizing markedly enhanced the corrosion resistance, increasing the total polarization resistance from 73.65 kΩcm^2 for the bare alloy to 7597 kΩcm^2 for the 14 μm coating and reducing the corrosion current density from 19.10 to 7.88 nAcm^2. Scanning electron microscopy with energy dispersive spectroscopy (SEM-EDS) revealed that the uncoated alloy experienced active dissolution and heterogeneous corrosion product formation, whereas the anodized samples formed a uniform, oxygen-enriched oxide layer that acted as an effective barrier against aggressive acidic species despite the presence of microcracks in the anodic layer. Atomic force microscopy (AFM) results further showed that increasing coating thickness decreased the surface roughness, with the Ra value decreasing from 50.213 nm for the bare alloy to 24.073 nm for the 14 μm coating, indicating improved surface stability under acidic conditions.

Keywords

AA6005, Anodized Coating Thickness, Corrosion, Simulated Acid Rain

1. Introduction

Among the types of degradation that metallic materials are exposed to throughout their service life, atmospheric corrosion stands out both for the scale of its impact and for the magnitude of its economic consequences. With the growth of industrialization and fossil fuel consumption, sulfur dioxide (SO_2) and nitrogen oxides (NOx) released into the atmosphere react with water vapor in clouds to form sulfuric and nitric acid compounds; these compounds then fall to the ground as rain, fog, or dew, creating the phenomenon known as "acid rain" [1]. While the pH of normal rainwater is around 5.6 when in equilibrium with atmospheric CO_2, the pH of acid rain measured in industrial areas can drop as low as 3.0 - 4.5. These low pH levels increase the ionic conductivity of thin electrolyte films that accumulate on metal surfaces, thereby accelerating the kinetics of electrochemical corrosion reactions [2].

Aluminum and its alloys are widely used in many engineering fields—particularly aerospace, automotive, rail systems, architectural facade cladding, and structural profile production—due to their low density, high strength-to-weight ratio, good workability, and relatively high corrosion resistance. The natural corrosion resistance of aluminum stems from a thin, dense Al_2O_3 layer that spontaneously forms on its surface; this layer partially isolates the underlying metal from direct exposure to atmospheric oxygen and moisture. However, this natural oxide layer can lose its stability under aggressive chemical conditions such as chloride ions or low-pH environments, which can lead to the initiation of localized pitting corrosion [3].

Dynamic electrochemical impedance spectroscopy (DEIS) studies conducted on 6060 and 6082 alloys have shown that AA6082, which has a higher Mn and Cr content, is more susceptible to pitting corrosion than AA6060, which contains lower amounts of alloying elements; this difference can be linked to the distribution of Al-rich phases within the alloy matrix [4]. The same studies emphasized that both alloys exhibited a distinct passive region in the simulated acid rain environment, although the passive current density varied depending on the alloy composition. Similarly, wet-dry cycle experiments conducted on 2024-T3 aluminum alloy using the electrochemical noise (EN) technique revealed that the corrosion process at low pH values such as 3.5 followed a much more severe and multi-stage course compared to pH 4.5 and 6.0; this can be explained by the high reactivity of hydrogen ions, their rapid diffusion/migration capability, and the reduced stability of the passive film at low pH [5].

One of the most widely used electrochemical surface treatments for increasing the corrosion resistance of aluminum alloys, improving surface hardness, and

providing aesthetic/decorative properties is anodic oxidation, commonly known as "anodizing" [6] [7]. In this process, the aluminum part is placed as the anode in an electrolytic cell, and a controlled Al_2O_3 layer is grown on the metal surface by applying direct current/voltage in electrolytes typically based on sulfuric acid, oxalic acid, or chromic acid. The anodic oxide film structure consists of a thin, dense "barrier layer" adjacent to the metal and a porous outer layer above it, composed of regular hexagonal cells; the barrier layer thickness, cell diameter, and pore diameter vary as a linear function of the applied anodizing voltage [8].

The effect of the anodized coating on corrosion resistance is closely related to the electrolyte composition and process parameters. Anodizing studies conducted on AA5052 alloy in a mixed citric acid-sulfuric acid electrolyte showed that increasing the citric acid concentration in the electrolyte (up to 70 g/L) increased the homogeneity and thickness of the oxide layer, which in turn significantly reduced the corrosion dissolution rate in the simulated acid rain environment [9]. This finding highlights that corrosion resistance depends not merely on the presence of the anodized coating, but also on its quality, including its thickness, homogeneity, and pore structure. On the other hand, a study comparing the corrosion performance of different surface treatments (sand-powder film coating, plain powder coating, hard anodized film, and conventional thermal sealing oxidation) on 6061 alloy in a 3.5% NaCl solution reported that the protective performance of all four coating types gradually decreased as the corrosion duration increased, with the protective ranking being: sand-powder film coating > hard anodized film > plain powder coating > conventional thermal sealing oxidation [10]. This result shows that anodized coatings do not provide absolute protection even under long-term exposure to aggressive environments, and that their time-dependent degradation behavior also needs to be characterized separately.

This study aims to contribute both to clarifying the corrosion mechanism of the anodized AA6005 alloy and to evaluating the reliable usability of this alloy in outdoor structural applications that may be exposed to acid rain. To this end, the corrosion behavior of uncoated AA6005 aluminum alloys and alloys with different anodized coating thicknesses was examined electrochemically in a simulated acid rain environment, and the changes occurring on the surface after the corrosion tests were investigated.

2. Materials and Method

2.1. Materials

The chemical composition of the AA6005 alloy used in this study is given in **Table 1**. The simulated acid rain employed in the corrosion tests was prepared in accordance with the composition outlined in the study by [11]. The final pH of the solution was adjusted/measured as 3.5. The required amounts of the individual components were dissolved in distilled/deionized water, and the solution was stirred until complete dissolution was achieved. The prepared solution was used immediately for the electrochemical corrosion tests.

Table 1. Chemical composition of AA6005 alloy.

Element	Si, wt. %	Mg, wt. %	Cu, wt. %	Mn, wt. %	Cr, wt. %
AA6005	0.60 - 1.0	0.40 - 0.60	≤0.10	≤0.10	≤0.10

2.2. Methods

For each experimental condition, five independent specimens were analyzed using OCP, EIS, Tafel polarization, SEM-EDS, and AFM techniques. For each technique, the measurement exhibiting the smallest deviation from the arithmetic mean of the five independent measurements was selected as the representative result and presented.

2.2.1. Anodizing Process

Before the anodizing process, the sample surfaces were polished using 800# - 2000# sandpaper. The anodizing process and subsequent post-anodizing treatments were performed using the conditions described below, with reference to DIN 17611[1]. The same treatment conditions were applied to all anodized specimens.

1) Degreasing bath: 60 - 70˚C, 5% detergent.

2) Caustic bath (NaOH): 55 - 70˚C operating temperature.

3) Neutralization: 20% sulfuric acid (H_2SO_4).

4) Anodizing bath: 20% sulfuric acid maintained at 18 ± 2˚C. The anodizing time was 30 min for the nominal 10 μm coating and 42 min for the nominal 14 μm coating.

5) Coloring: Tin sulfate ($SnSO_4$), 20˚C.

6) Yellow bath: Ferric ammonium oxalate, 55˚C.

7) Hot sealing: 98˚C in distilled water for 30 min and 42 min for the nominal 10 μm and 14 μm coatings, respectively.

2.2.2. Electrochemical Impedance Spectroscopy (EIS)

The EIS experiments were carried out using a three-electrode system, with Ag/AgCl as the reference electrode, platinum as the counter electrode, and AA6005 with a surface area of 0.636 cm^2 as the working electrode. Before each experiment, the working electrode was immersed in the test solutions at 25˚C for 1 hour in order to obtain a stable open circuit potential (OCP). The EIS measurements were performed using a 10 mV amplitude signal over a frequency range of 0.1 Hz - 100 kHz. The obtained data were analyzed using the ZsimpWin 3.21 software.

2.2.3. Tafel Polarization (TP)

The TP experiments were carried out immediately after the EIS measurements. Tafel polarization tests were performed in the same three-electrode cell used for EIS, with Ag/AgCl as reference and a platinum counter electrode. The working electrode was scanned first in the cathodic and then in the anodic direction, over

[1]DIN 17611 (2022) Anodized products of wrought aluminium and wrought aluminium alloys—Technical conditions of delivery. Deutsches Institut für Normung (DIN), Berlin, Germany. https://doi.org/10.31030/3365090

a potential range of −0.5 to +1.5 V relative to E_{corr}, at a scan rate of 1 mV/s. No iR compensation was applied to the polarization data. The Tafel parameters were determined by the instrument software from the linear regions of the anodic and cathodic branches around E_{corr}.

2.2.4. Surface Analysis

The surface morphologies formed after the corrosion tests were analyzed in detail using SEM (FEI Quanta FEG 250, the Netherlands) and AFM (Park Systems, XE-100E) instruments.

3. Results

3.1. Open Circuit Potential (OCP)

Figure 1 shows the open circuit potential (OCP) plots of uncoated and anodized AA6005 metals exposed to the simulated acid rain environment.

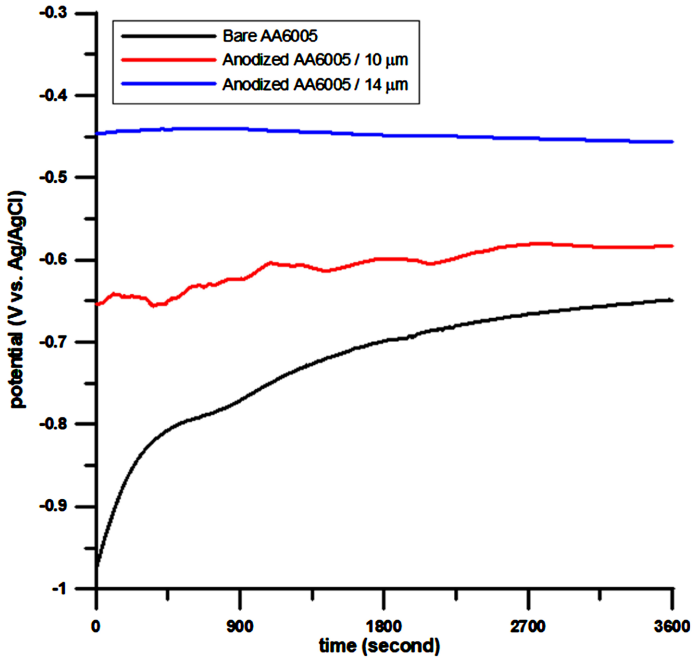

Figure 1. OCP graph of AA6005 metals exposed to the acid rain environment.

When Figure 1 is examined, it can be seen that the corrosion potential of the uncoated AA6005 metal starts from a more negative value compared to the anodized metals. The potential of the uncoated AA6005 metal shifted in the positive direction during the first 900 seconds and then became stable. This indicates the gradual formation of either a corrosion product layer or a partially protective oxide film. When the anodized AA6005 metals are examined, their potentials are seen to be more stable than that of the uncoated metal. It was determined that the corrosion potential also shifted in the positive direction as the anodized coating thickness increased. According to the OCP data, the nominal 14 µm anodized coating exhibited the most positive and stable potential among the investigated

coating thicknesses, indicating improved protection of the underlying aluminum substrate against the aggressive species present in the simulated acid rain environment (H^+, SO_4^{2-}, NO_3^-, etc.).

3.2. Electrochemical Impedance Spectroscopy (EIS)

Figure 2 shows the Nyquist and Bode plots obtained from the EIS measurements of uncoated and anodized AA6005 metals exposed to the simulated acid rain environment.

When the Nyquist diagrams in Figure 2(a) are examined, it can be seen that the uncoated AA6005 sample exhibits a smaller-diameter semicircle compared to the anodized samples. A smaller semicircle indicates lower charge transfer resistance and faster corrosion of the metal. In the anodized metals, the Nyquist curves reach much higher impedance values. The nominal 14 μm coating exhibited the highest impedance among the investigated specimens, as shown in Figure 2(a). The Bode and phase angle diagrams given in Figure 2(b) support the Nyquist plots. Table 2 presents the EIS test results analyzed using the $R(QR)$ and $R(QR)(QR)$ circuit models for the Nyquist curves.

Table 2 shows that the anodizing process substantially improves the corrosion resistance of AA6005 metal in the simulated acid rain environment. While the corrosion resistance (R_{total}) of the uncoated AA6005 metal was 73.65 kΩcm^2, it was determined that this value increased to 3554 and 7597 kΩcm^2 respectively in the anodized metals. In addition, the decrease observed in the Q_f and Q_{dl} values indicates the formation of a more compact and less porous oxide layer. The increase in the n values indicates that the anodized layer exhibits a more homogeneous and near-ideal capacitive behavior. According to the data obtained from EIS, it was determined that the anodizing process slows down the transport of aggressive ions present in the simulated acid rain to the metal surface, and that a more protective layer forms as the coating thickness increases.

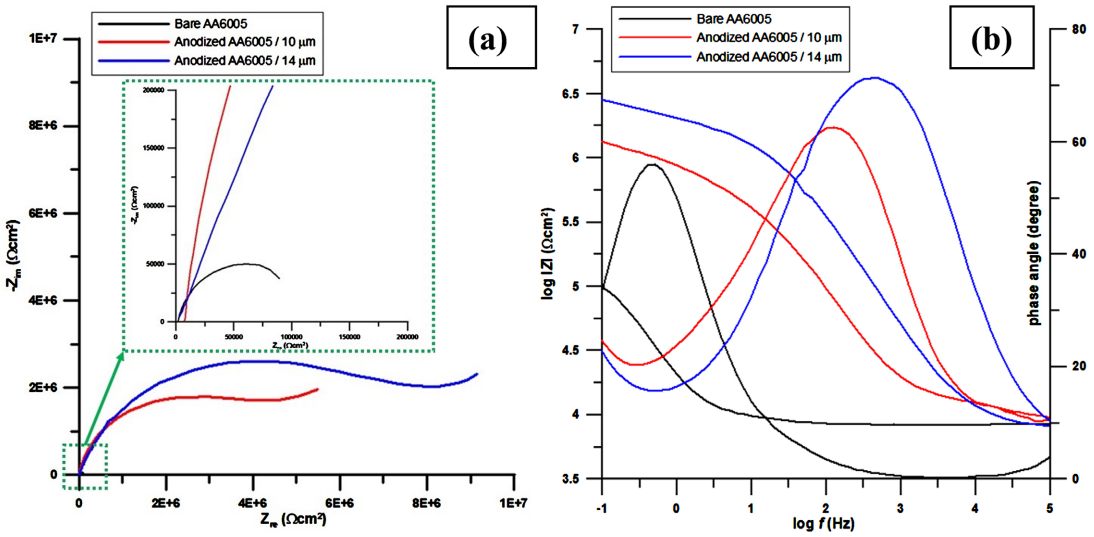

Figure 2. EIS graphs of AA6005 metals exposed to the acid rain environment; (a) Nyquist, (b) Bode.

Table 2. EIS test results of AA6005 metals exposed to the acid rain environment.

	R_s (Ωcm^2)	Q_f		R_f ($k\Omega cm^2$)	Q_{dl}		R_{ct} ($k\Omega cm^2$)	R_{total} ($k\Omega cm^2$)	Chi-square
		Y_0 ($\Omega^{-1}S^n cm^{-2}$)	$0 \leq n_f \leq 1$		Y_0 ($\Omega^{-1}S^n cm^{-2}$)	$0 \leq n_{dl} \leq 1$			
Bare AA6005	1215	-	-	-	1.07E−05	0.89	73.65	73.65	7.090e−05
Anodized AA6005/10 μm	1206	4.26E−07	0.81	2017	1.99E−07	0.91	1537	3554	2.404e−04
Anodized AA6005/14 μm	1239	1.23E−08	0.85	3458	3.73E−08	0.92	4139	7597	4.508e−04

3.3. Tafel Polarization (TP)

Figure 3 shows the plots obtained from the TP measurements of uncoated and anodized AA6005 metals exposed to the simulated acid rain environment.

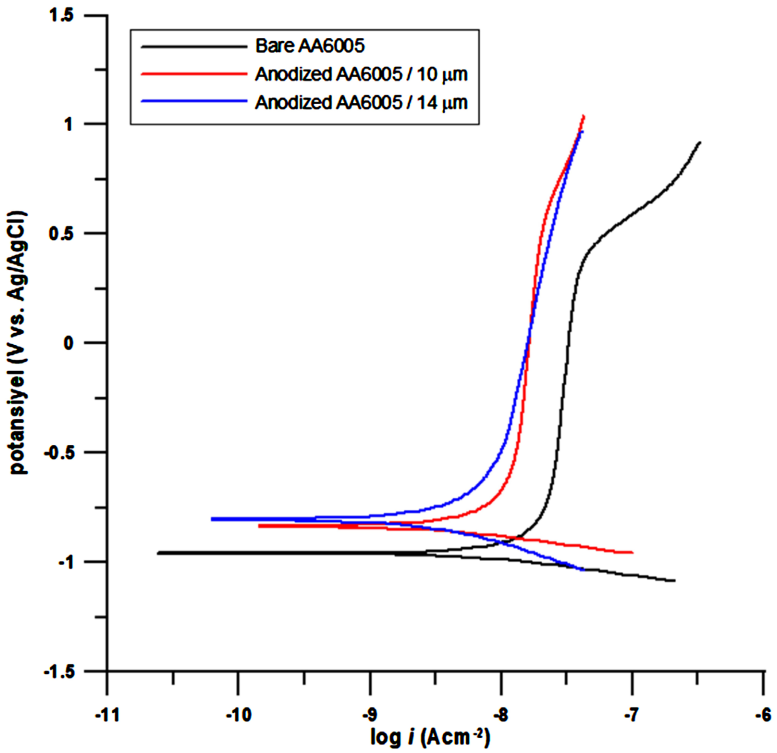

Figure 3. TP graphs of AA6005 metals exposed to the acid rain environment.

The TP curves given in Figure 3 show that anodizing substantially improves the corrosion resistance of AA6005 metal. It can be seen that the corrosion current densities of the anodized metals are lower compared to the uncoated AA6005 metal. In particular, the AA6005 specimen with the nominal 14 μm coating exhibited the lowest corrosion current density among the investigated specimens. The data obtained from the TP method are given in Table 3.

According to the data in Table 3, it can be seen that the anodizing process increases the corrosion resistance of AA6005 metal. While the corrosion current

density (i_{corr}) of the uncoated AA6005 metal was 19.10 nA/cm^2, it was determined that this value decreased to 8.93 and 7.88 nA/cm^2 respectively in the anodized metals. The TP results support the EIS findings, showing that the nominal 14 μm coating provided better corrosion protection than the nominal 10 μm coating under the investigated conditions.

Table 3. TP test results of AA6005 metals exposed to the acid rain environment.

	β_a (mV/dec)	β_c (mV/dec)	E_{corr} (mV)	i_{corr} (nA/cm^2)
Bare AA6005	456	110	−957	19.10
Anodized AA6005/10 μm	450	140	−832	8.93
Anodized AA6005/14 μm	447	177	−803	7.88

3.4. Surface Analysis

Figure 4 shows the cross-sectional SEM images and EDS analysis results of uncoated and anodized AA6005 metals.

When Figure 4(a) and Figure 4(b) are examined, the average coating thicknesses are seen to be approximately 10 μm and 13.5 μm respectively, and the resulting oxide layer is seen to be well integrated with the Al substrate. The EDS-1 analysis obtained from the coating layer showed that the surface was predominantly composed of Al (41.5%) and O (56.6%), supporting the formation of an A-O-rich anodic oxide layer. The detected S content (1.8%) is consistent with the use of a slfuric acid-based anodizing electrolyte. The EDS-2 analysis taken from the base metal, on the other hand, confirmed the chemical composition of the AA6005 aluminum matrix through the absence of an O peak and the presence of Mg (1.4%), Si (0.3%), and Fe (0.2%) elements. Figure 5 presents the SEM images and EDS analysis results taken from the surface after the corrosion tests.

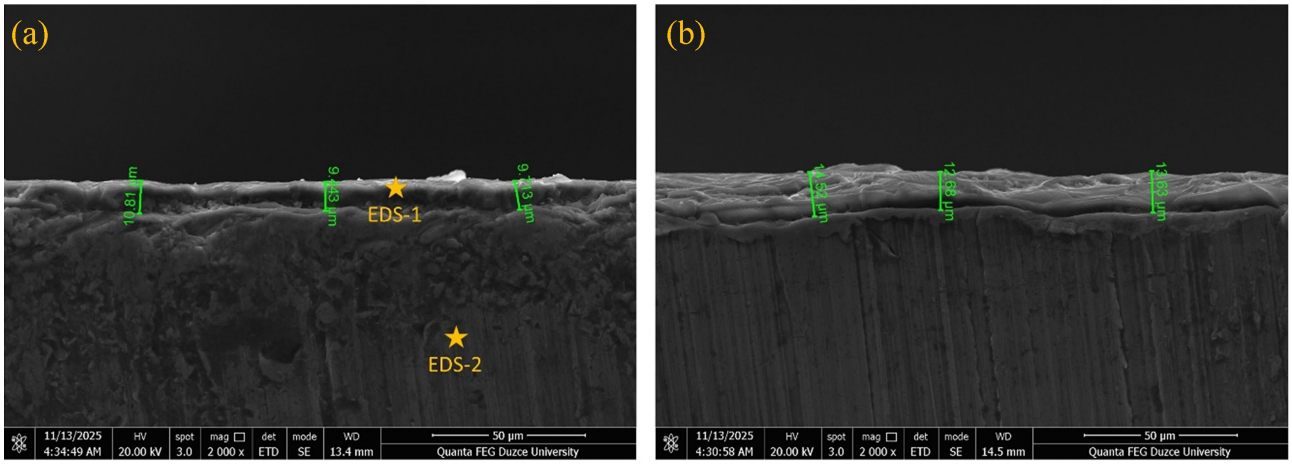

	Mg	Al	Si	Fe	O	S
EDS-1	-	41.5	-	-	56.6	1.8
EDS-2	1.4	98.1	0.3	0.2	-	-

Figure 4. Cross-sectional SEM images and EDS results of uncoated and anodized AA6005 metals; (a) 10 μm, (b) 14 μm.

Comparative analysis of the SEM images indicates that the applied coating improves the corrosion resistance against the simulated acid rain environment. In the SEM images of the uncoated sample (**Figure 5(a)**), irregularly distributed, porous, and heterogeneous corrosion product accumulations were observed on the surface; this indicates that the substrate underwent active electrochemical dissolution by directly interacting with the acidic environment and that localized corrosion regions formed on the surface. When the images of the coated samples are examined, no obvious corrosion products were observed, but cracks were observed in the anodized coating layer (**Figure 5(b)** and **Figure 5(c)**). The cracks that formed on the surface may originate from surface stresses caused by the growth of the anodized layer and/or from the thermal shock that occurs when transitioning to the 98˚C bath during the anodizing process [12]. When comparing the coatings with 10 µm (**Figure 5(b)**) and 14 µm (**Figure 5(c)**) thickness, the crack density and cell frequency were found to be relatively higher in the thinner coating (**Figure 5(b)**), which is thought to be related to the increasing stress-to-thickness ratio as the film

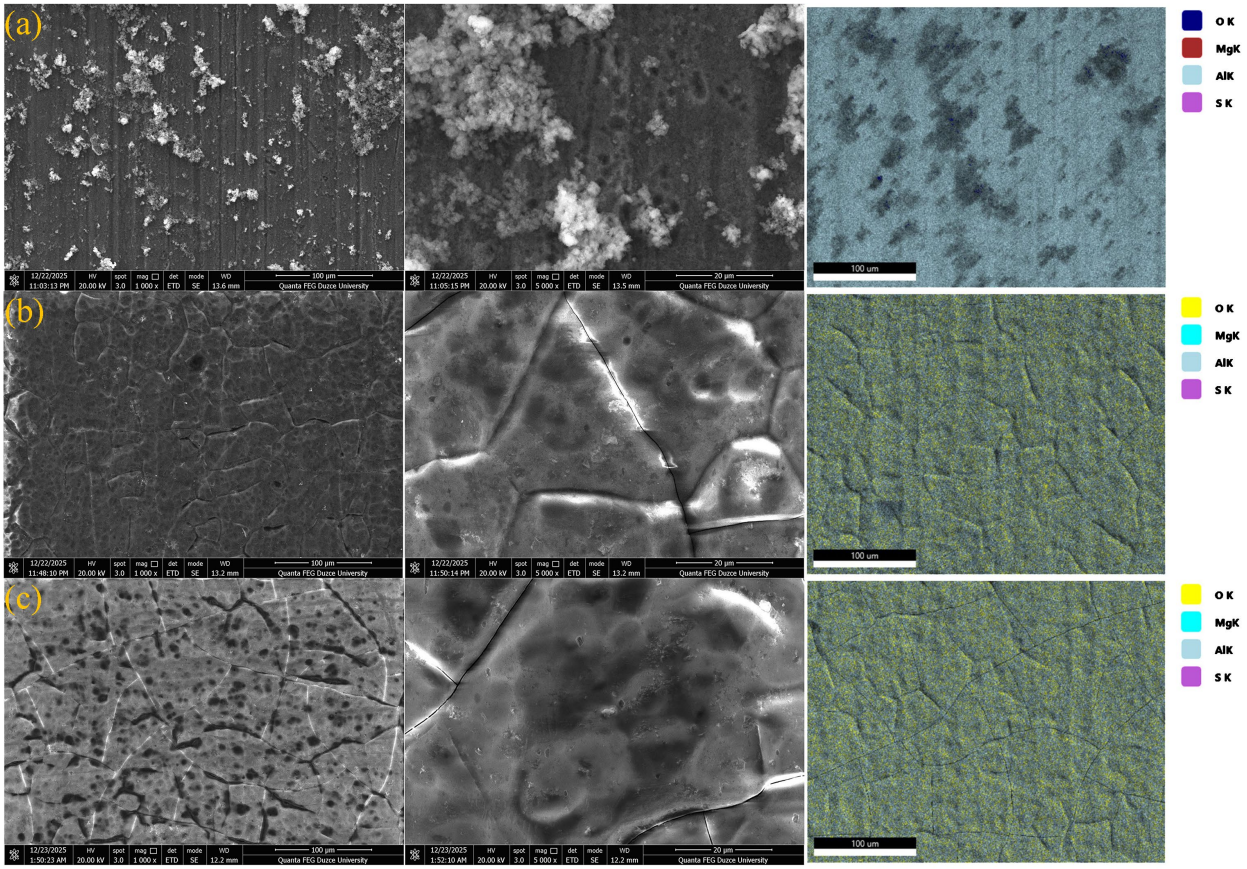

	O	Mg	Al	S
Bare AA6005	25.4	1.0	72.8	0.8
Anodized AA6005 / 10 µm	58.1	0.6	37.1	4.3
Anodized AA6005 / 14 µm	59.6	0.6	36.0	3.7

Figure 5. Post-corrosion SEM images and EDS results of uncoated and anodized AA6005 metals; (a) uncoated, (b) 10 µm, (c) 14 µm.

thickness decreases. The absence of significant corrosion product accumulation on the substrate surface in both coated samples indicates that the coating forms an effective barrier layer that limits the access of acidic species to the substrate. Even though both anodized layers showed tiny cracks, the 14 μm layer offered better protection against aggressive ions, suggesting that the thicker coating improved the overall defense capability, despite the existence of surface fractures.

The EDS elemental mapping and point analysis results quantitatively confirm the presence of the coating and the compositional changes, supporting the morphological observations. While the oxygen content was measured at 25.4% in the uncoated AA6005 sample, this value increased to 58.1% for the 10 μm coating and 59.6% for the 14 μm coating in the anodized samples; in contrast, the aluminum ratio decreased from 72.8% in the uncoated sample to approximately 36 - 37% in the coated samples. The approximately twofold increase in oxygen content and the marked decrease in the aluminum signal indicate that the anodized coating forms a continuous barrier layer of sufficient thickness on the surface. The elemental mapping results also support this finding: the O K signal showed a homogeneous distribution on the surface in the coated samples, whereas the Al K signal was dominant in the uncoated sample, with signal weakening observed in regions containing corrosion product accumulations. Regarding the changes in S ratio, while the S ratio was 0.8% in the uncoated sample, this ratio increased to 4.3% (10 μm) and 3.7% (14 μm) in the coated samples. A previous study reported that when anodizing is carried out in a sulfuric-acid-based environment, it is difficult to determine whether the S element detected by EDS originates from a corrosion product or from the chemical composition of the coating, and therefore foreign elements should be examined instead. The absence of foreign elements in the obtained EDS results suggests that the S element originates from the chemical composition of the coating. Overall, the SEM-EDS findings are consistent with the electrochemical results, indicating that the nominal 14 μm coating provided better protection than the nominal 10 μm coating under the investigated conditions. Figure 6 presents the AFM analysis results obtained from the surfaces after the corrosion tests.

The AFM results reveal clear differences in the surface topography of uncoated and anodized AA6005 alloys after exposure to the simulated acid rain environment. The R_a and R_z values of the uncoated AA6005 alloy were determined to be 50.213 nm and 143.138 nm, respectively. In the anodized samples (10 μm and 14 μm), the R_a values decreased to 38.075 nm and 24.073 nm, respectively, while the R_z values decreased to 100.040 nm and 92.874 nm. This decrease indicates that, compared to uncoated aluminum, the anodized coating delays the increase in surface roughness in the aggressive environment and protects the metal against corrosion.

4. Conclusions

The present study is concerned with the evaluation of the corrosion behavior of uncoated and anodized AA6005 aluminum alloys within a simulated acid rain environment. The principal findings are summarized as follows:

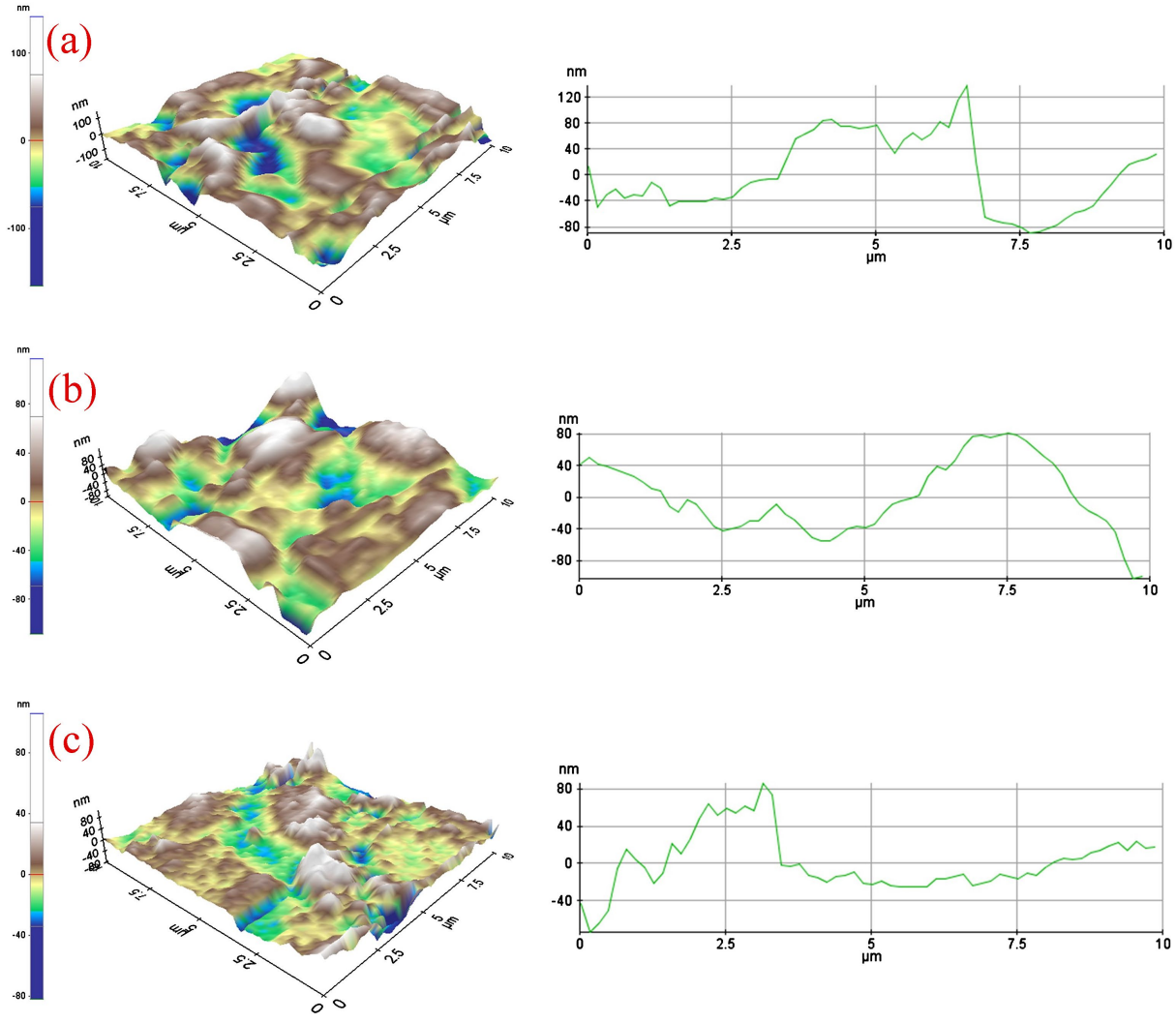

	R_a (nm)	R_z (nm)
Bare AA6005	50.213	143.138
Anodized AA6005 / 10 μm	38.075	100.040
Anodized AA6005 / 14 μm	24.073	92.874

Figure 6. Post-corrosion AFM results of uncoated and anodized AA6005 metals; (a) uncoated, (b) 10 μm, (c) 14 μm.

1) Anodizing substantially improves the corrosion resistance of the AA6005 alloy. The nominal 14 μm coating demonstrated the most robust protective behavior, as evidenced by the shift in the OCP to more noble values, an increase in total impedance (Rtotal) from 73.65 kΩcm^2 to 7597 kΩcm^2, and a reduction in the corrosion current density (icorr) from 19.10 nA/cm^2 to 7.88 nA/cm^2.

2) The results of the SEM-EDS analyses demonstrate that whilst uncoated samples undergo active dissolution with subsequent corrosion product accumulation, the anodized coatings form a homogeneous, continuous and oxygen-rich barrier layer that effectively isolates the underlying substrate.

3) AFM measurements demonstrate a substantial decrease in surface roughness subsequent to anodization. The average surface roughness (R_a) of the uncoated alloy was measured at 50.213 nm, whereas the 14 μm coated sample exhibited an average surface roughness of 24.073 nm. This reduction in surface roughness suggests that the coating process minimizes the physical adsorption of aggressive ions, thereby creating a smoother surface.

4) Based on the electrochemical and surface characterization results obtained in this study, the nominal 14 μm anodized coating exhibited the highest corrosion resistance among the investigated coating thicknesses. However, a broader range of coating thicknesses should be investigated to determine the optimum thickness for specific service conditions.

5) Future research should systematically investigate a wider range of anodic coating thicknesses to establish the optimum coating thickness for different service conditions. Dynamic Electrochemical Impedance Spectroscopy (DEIS) is recommended to monitor the time-dependent evolution of the anodic oxide layer and its degradation mechanisms, while long-term exposure tests under both simulated and natural atmospheric environments should be conducted to validate the durability and corrosion performance of anodized AA6005 alloys.

Author Contributions

Conceptualization, Eren Saray, Fatma Zehra Arı, and Demet Giyik; methodology, Eren Saray and Mesut Yıldız; investigation, Eren Saray, Fatma Zehra Arı, and Demet Giyik; formal analysis, Eren Saray and Mesut Yıldız; writing—original draft preparation, Eren Saray; writing—review and editing, Hüsnü Gerengi, Mesut Yıldız, Fatma Zehra Arı, and Demet Giyik; supervision, Hüsnü Gerengi; project administration, Hüsnü Gerengi; funding acquisition, Hüsnü Gerengi. All authors have read and agreed to the published version of the manuscript.

Acknowledgements

The authors gratefully acknowledge the financial support provided by the Düzce University Research Fund (Project No. 2025.06.05.1611). The experimental work was further supported by a university-industry collaboration carried out within the framework of the TÜBİTAK 1707 Program (Project No. 3255014).

Conflicts of Interest

The authors declare no conflicts of interest regarding the publication of this paper.

References

[1] Gaddamwar, A.G. (2011) Analytical Study of Rain Water for the Determination of Polluted or Unpolluted Zone. *International Journal of Environmental Sciences*, **1**, 1317-1322.

[2] Pilić, Z. and Martinović, I. (2017) A Comparative Study on the Electrochemical Behaviour of Aluminium and 8090 Al-Li-Cu-Mg Alloy in Acid Rain Solution. *Interna-*

tional Journal of Electrochemical Science, **12**, 3576-3588. https://doi.org/10.20964/2017.05.46

[3] Alqarni, N., El-Gammal, B., Fawzy, A., Bahir, A.A. and Toghan, A. (2022) Investigation of Expired Ticarcillin and Carbenicillin Drugs for Inhibition of Aluminum Corrosion in Hydrochloric Acid Solution. *International Journal of Electrochemical Science*, **17**, Article 2212113. https://doi.org/10.20964/2022.12.99

[4] Gerengi, H., Slepski, P., Ozgan, E. and Kurtay, M. (2013) Investigation of Corrosion Behavior of 6060 and 6082 Aluminum Alloys under Simulated Acid Rain Conditions. *Materials and Corrosion*, **66**, 233-240. https://doi.org/10.1002/maco.201307287

[5] Shi, Y., Zhang, Z., Su, J., Cao, F. and Zhang, J. (2006) Electrochemical Noise Study on 2024-T3 Aluminum Alloy Corrosion in Simulated Acid Rain under Cyclic Wet-Dry Condition. *Electrochimica Acta*, **51**, 4977-4986. https://doi.org/10.1016/j.electacta.2006.01.050

[6] Paz Martínez-Viademonte, M., Abrahami, S.T., Hack, T., Burchardt, M. and Terryn, H. (2020) A Review on Anodizing of Aerospace Aluminum Alloys for Corrosion Protection. *Coatings*, **10**, Article 1106. https://doi.org/10.3390/coatings10111106

[7] Carreira, A.F., Pereira, A.M., Vaz, E.P., Cabral, A.M., Ghidini, T., Pigliaru, L., *et al.* (2017) Alternative Corrosion Protection Pretreatments for Aluminum Alloys. *Journal of Coatings Technology and Research*, **14**, 879-892. https://doi.org/10.1007/s11998-017-9922-9

[8] Iqbal, M.A., Sun, L., Barrett, A.T. and Fedel, M. (2020) Layered Double Hydroxide Protective Films Developed on Aluminum and Aluminum Alloys: Synthetic Methods and Anti-Corrosion Mechanisms. *Coatings*, **10**, Article 428. https://doi.org/10.3390/coatings10040428

[9] Gu, J., Zhang, X. and Yu, L. (2023) Investigation on Anodized 5052 Aluminum Alloy and Its Corrosion Resistance in Simulated Acid Rain. *International Journal of Electrochemical Science*, **18**, Article 100336. https://doi.org/10.1016/j.ijoes.2023.100336

[10] Fan, L., Wang, F., Wang, Z., Hao, X., Yang, N. and Ran, D. (2023) Study on the Influence of Surface Treatment Process on the Corrosion Resistance of Aluminum Alloy Profile Coating. *Materials*, **16**, Article 6027. https://doi.org/10.3390/ma16176027

[11] Gerengi, H., Bereket, G. and Kurtay, M. (2016) A Morphological and Electrochemical Comparison of the Corrosion Process of Aluminum Alloys under Simulated Acid Rain Conditions. https://doi.org/10.1016/j.jtice.2015.05.023

[12] Miramontes, J.C., Gaona Tiburcio, C., García Mata, E., Esneider Alcála, M.Á., Maldonado-Bandala, E., Lara-Banda, M., *et al.* (2022) Corrosion Resistance of Aluminum Alloy AA2024 with Hard Anodizing in Sulfuric Acid-Free Solution. *Materials*, **15**, Article 6401. https://doi.org/10.3390/ma15186401